Proceedings of DETC'03
ASME 2003 Design Engineering Technical Conferences and
Computers and Information in Engineering Conference
Chicago, Illinois, USA, September 2-6, 2003

DETC2003/DAC-48753

PARAMETRIC DESIGN SENSITIVITY ANALYSIS OF HIGH FREQUENCY STRUCTURAL-ACOUSTIC PROBLEMS USING ENERGY FINITE ELEMENT METHOD

Kyung K. Choi and Jun Dong
Center for Computer-Aided Design and
Department of Mechanical & Industrial Engineering
The University of Iowa
Iowa City, IA 52242, USA
kkchoi@ccad.uiowa.edu, jundong@ccad.uiowa.edu

Nickolas Vlahopoulos, Aimin Wang, Weiguo Zhang
Department of Naval Architecture and Marine Engineering
The University of Michigan
Ann Arbor, MI 48109, USA
nickvl@engin.umich.edu, wangam@engin.umich.edu,
zhangwg@engin.umich.edu

ABSTRACT

A design sensitivity analysis of high frequency structural-acoustic problem is formulated and presented. The Energy Finite Element Method (EFEM) is used to predict the structural-acoustic responses in high frequency range, where the coupling between the structural and acoustic domain are modeled by using radiation efficiency. The continuum design sensitivity formulation is derived from the governing equation of EFEM and the discrete method is applied in the variation of the structural-acoustic coupling matrix. The direct differentiation and adjoint variable method are both developed for the sensitivity analysis, where the difficulty of the adjoint variable method is overcome by solving a transposed system equation. Parametric design variables such as panel thickness and material damping are considered for sensitivity analysis, and the numerical sensitivity results show excellent agreement comparing with the finite difference results.

KEYWORDS

Structural Acoustics, Design Sensitivity Analysis (DSA), Energy Finite Element Method (EFEM), Adjoint Variable Method, Radiation Efficiency

1. INTRODUCTION

Structure induced sound and vibration has been a concern for scientists and engineers for a long time. How to precisely predict the structural-acoustic response and design structures for the best acoustic comfort with least usage of materials have allured thorough research in this area. Finite Element Method (FEM) and Boundary Element Method (BEM) are favorite choices in solving structural-acoustic problems. Atalla and Bernhard [1] summarized the application of FEM and BEM in the low frequency structural-acoustic analysis. Numerous applications [2-5] have already promoted FEM and BEM an industrial standard in Computer Aided Engineering (CAE).

For the Design Sensitivity Analysis (DSA) using FEM and BEM, a lot of research has been done in different applications. Ma and Hagiwara [6] derived an eigenvalue and eigenvector sensitivity formulation for acoustic-structural coupled problem using FEM; Smith and Bernhard [7] developed a shape sensitivity formulation of using BEM in radiation problem. Choi et al. [8,9] developed the continuum sensitivity formulation for coupled structural-acoustic problem using FEM and applied it to optimization of passenger vehicles. Kim et al. [10] developed an adjoint variable method for a sequential structural-acoustic problem using FEM and BEM, which is then used by Dong et al. [11] in the design optimization of a complex vehicle structure for minimum weight.

Unfortunately, FEM or BEM cannot always assure to be efficient and accurate, especially for high frequency range, where the structural response is extremely sensitive to the design change. In order to capture the structural characteristic length, much smaller mesh size is required for the FEM or BEM model, and thus making it computationally expensive or even prohibitive. Nefske et al. [12] investigated the requirement of the element size for FEM to be accurate in dynamic analysis, Bernhard [1] recommended that at least six linear elements or three quadratic elements should be required per wavelength for an accurate analysis, and thus it is commonly agreed that FEM and BEM could only be suitable for the problem with frequency up to 200 Hz.

The difficulty of applying FEM and BEM in high frequency range forced researchers look for an alternative method. Lyon [13] and Maidanik [14] developed Statistical Energy Analysis (SEA) using a modal based approach that is suitable for high frequency problems. Due to its easy-to-understand nature, SEA has been widely accepted as an analysis tool in practice,

especially for large-scale structures. The work done by Chen [15,16] in SEA analysis and experimental validation of a full vehicle structure to predict the energy flow in the vehicle is one of typical applications.

Although SEA seems suitable to solve high frequency problems, its inherent weakness is that it is based on the division of sub-structures such that the local modeling details are ignored. This weakness keeps SEA away from being a good design tool for structural details. In order to overcome this disadvantage, Nefske and Sung [17], Wohlever and Bernhard [18], Bouthier and Bernhard [19,20,21] developed the governing equation for the time and space averaged energy flow between coupled structures using a wave approach, which is then combined with finite element discretization to form the foundation of the Energy Finite Element Method (EFEM). EFEM had not been very successful to implement until Langley and Heron [22] developed an analytical method to evaluate the power transfer coefficient between structural members, and Cho [23] developed a formulation to construct the coupling matrix based on the power flow conservation between the coupled structures.

Since then, EFEM has been successfully applied to various engineering problems. Vlahopoulos et al. [24,25] validated EFEM by applying it to a complex ship structure comparing with SEA and dense FEA results. Wang [26] used a degenerated version of EFEM to analyze the cabin of the heavy-duty truck.

While the structural-structural EFEM has been successfully developed and applied to high frequency problems, the structural-acoustic EFEM has not been investigated until Bitsie [27] derived the coupling relationship between structural and acoustic domains based on the definition of radiation efficiency. Zhang and Wang [28] extended EFEM to consider the fluid loading on the structural vibration at high frequency. They also investigated the effect of the structural radiation damping on the EFEM governing equation.

The flexibility and accuracy of EFEM makes it one of the best choices in solving high frequency structural-acoustic problems. In order to carry out design optimization using EFEM, the sensitivity of EFEM also needs to be developed. Comparing with the research efforts which have been done in the high-frequency structural-acoustic analysis, not much work has been done in design sensitivity analysis. Bitsie and Bernhard [27,31] discussed sensitivity of the energy density with respect to the material damping, but no rigorous and detailed sensitivity formulation was derived. Borlase and Vlahopoulos [32] carried out a design optimization of a naval structure using EFEM, but the gradient is obtained using the finite difference rather than sensitivity calculation.

Kim et al. [33] developed a rigorous parametric and shape design sensitivity formulation for structural systems using EFEM, but the structural-acoustic relationship has not been addressed. This paper presents a discussion on the structural-acoustic relationship in EFEM and a detailed derivation of the parametric sensitivity formulation for the structural-acoustic coupled problem. Both direct differentiation and adjoint variable methods are developed and tested using two examples, and excellent agreements are observed between sensitivity and finite difference results.

2. ENERGY FINITE ELEMENT METHOD FOR HIGH FREQUENCY STRUCTURAL-ACOUSTIC PROBLEM

2.1 Energy Finite Element Method (EFEM)

The governing equation for EFEM was derived by Nefske and Sung for beams [17], Bouthier and Bernhard for plates [19,20,21], and Bitsie for acoustic space [27]. Consider a coupled structural-acoustic domain as shown in Fig. 1, where the governing equations for the structural and acoustic domains can be written, respectively, in the form of

$$-\frac{c_g^2}{\eta_s \omega}\nabla^2 e_s + \eta_s \omega e_s = \pi_s \text{, on } \Omega_s \tag{1}$$

$$-\frac{c^2}{\eta_a \omega}\nabla^2 e_a + \eta_a \omega e_a = \pi_a \text{, on } \Omega_a \tag{2}$$

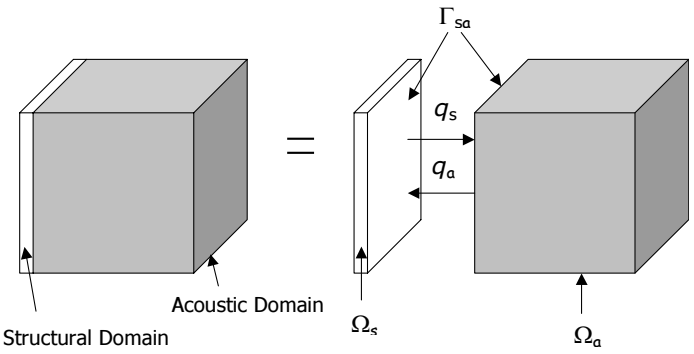

Figure 1. Structural-Acoustic Coupled Domain

In the governing Eqs. (1) and (2), c_g is the structural group velocity, c is the air speed, η_s and η_a are the hysteresis damping factors for the structure and air respectively, ω is the radian frequency of structural vibration. The power flow input to the structural and acoustic domains are denoted by π_s and π_a, respectively. The primary variables e_s and e_a, which are the time and space averaged energy density, are used to characterize the structural-acoustic behavior. The governing Eqs. (1) and (2) describe the energy conservation in both structural and acoustic domains: the incoming energy flow equals to the energy dissipated in the system and energy transmitted across the structural boundaries.

Governing Eqs. (1) and (2) are valid only if the structure and air do not affect each other except the power flow at the interface. However, the structural dynamic characteristics are influenced by the contacted fluid, and this effect needs to be included in the governing equation of structural vibration. Zhang et al. [28] pointed out that the effect of the fluid loading on the structural vibration differs by the coincidence frequency f_c, at which the structural bending wave number k_f coincides with the acoustic wave number k. For the frequency above the coincidence frequency, the effect can be expressed in terms of the radiation damping factor. For the frequency below the coincidence frequency, the effect is expressed in terms of the effective surface mass density (or the effective group bending velocity) and the radiation damping factor. Thus, Eq. (1) is changed to

$$-\frac{c_g^2}{\left(\eta_s + \eta_{rad}\right)\omega}\nabla^2 e_s + \left(\eta_s + \eta_{rad}\right)\omega e_s = \pi_s \tag{3}$$

where η_{rad} is called the radiation damping, which characterizes the capacity of the plate to radiate acoustic energy, defined as

$$\eta_{rad} = \left(\frac{\rho_0}{\rho_S}\right)\frac{1}{\alpha k h}\sigma_{rad} \tag{4}$$

In Eq. (4), the structural bending group speed can be computed via the formulation $c_g=2(D\omega^2/\alpha\rho_s h)^{1/4}$, where D is the flexural rigidity of the plate, with $\alpha=1$ for the frequency ω above the coincidence frequency and $\alpha=1+\rho_0/\rho_s h(k_f^2-k^2)^{1/2}$ for ω below the coincidence frequency.

Equation (4) shows that the radiation damping is a function of the structural thickness h, structural mass density ρ_s, fluid mass density ρ_0, and σ_{rad}, which is defined as radiation efficiency, reflecting the interaction between the bending vibration of the structure and fluid. The numerical model to evaluate σ_{rad} is discussed in section 2.2.

The variational form of the governing Eqs. (2) and (3) can be obtained by multiplying both sides by the virtual energy density $\overline{e}_s \in Z_s$ and $\overline{e}_a \in Z_a$, respectively, integrating over the structural domain Ω_s and acoustic domain Ω_a, respectively, applying divergence theorem, and imposing the interface power flow conservation $q_s + q_a = 0$ as

$$a_{\Omega_s}(e_s,\overline{e}_s) + b_{\Gamma_{sa}}(e_s,e_a,\overline{e}_s,\overline{e}_a) + d_{\Omega_a}(e_a,\overline{e}_a) = \ell_{\Omega_s}(\overline{e}_s) + p_{\Omega_a}(\overline{e}_a) \quad \forall\, \overline{\boldsymbol{e}} \in Z \tag{5}$$

where the subscripts denote the physical domains on which the integration is taken.

The above variational equation will hold for all kinematically admissible virtual energy density $\overline{\boldsymbol{e}} = \{\overline{e}_s, \overline{e}_a\} \in Z$, where Z is the space defined as

$$Z = \left\{ \boldsymbol{e} = (e_s, e_a) \in Z_s \times Z_a \mid q_s + q_a = 0 \ \text{ on } \ \Gamma_{sa} \right\} \tag{6}$$

with

$$Z_s = \left\{ e_s \mid e_s \in [H^0(\Omega_s)]^2, q_s = 0 \ \text{ on } \ \Gamma_s^g, q_s = \hat{q}_s \ \text{ on } \ \Gamma_s^h \right\} \tag{7}$$

$$Z_a = \left\{ e_a \mid e_a \in [H^0(\Omega_a)]^2, q_a = 0 \ \text{ on } \ \Gamma_a^g, q_a = \hat{q}_a \ \text{ on } \ \Gamma_a^h \right\} \tag{8}$$

and q_s and q_a are the power flow along Γ_{sa}, which is the interface between the structural and acoustic domains. In Eq. (7) and (8), H^0 is the Sobolev space of order zero [34].

In the variational equation, $a_{\Omega_s}(e_s,\overline{e}_s)$ and $d_{\Omega_a}(e_a,\overline{e}_a)$ are the energy bilinear forms for structural and acoustic domains respectively, $\ell_{\Omega_s}(\overline{e}_s)$ is the structural load linear form, $p_{\Omega_a}(\overline{e}_a)$ is the acoustic load linear form, $b_{\Gamma_{sa}}(e_s,e_a,\overline{e}_s,\overline{e}_a)$ is the coupling term between the structural and acoustic domains sharing the common boundary Γ_{sa}. It should be noted that the coupling term exists along the structural discontinuities as well. However, for the sake of structural-acoustic design sensitivity analysis, only the coupling between structural and acoustic domains will be investigated. The detailed discussion of the structural-structural coupling relationship and parametric and shape design sensitivity formulation can be found in Kim et al. [33].

The definition of the continuum energy bilinear and load linear forms in the variational equation is:

$$a_{\Omega_s}(e_s,\overline{e}_s) \equiv \iint_{\Omega_s}\left[\frac{c_g^2}{(\eta_s+\eta_{rad})\omega}\nabla\overline{e}_s\cdot\nabla e_s + (\eta_s+\eta_{rad})\omega\,\overline{e}_s e_s\right]d\Omega \tag{9}$$

$$d_{\Omega_a}(e_a,\overline{e}_a) \equiv \iint_{\Omega_a}\left(\frac{c^2}{\eta_a\omega}\nabla\overline{e}_a\cdot\nabla e_a + \eta_a\omega\,\overline{e}_a e_a\right)d\Omega \tag{10}$$

$$b_{\Gamma_{sa}}(e_s,e_a,\overline{e}_s,\overline{e}_a) \equiv \int_{\Gamma_{sa}}(\overline{e}_s q_s + \overline{e}_a q_a)\,d\Gamma \tag{11}$$

$$\ell_{\Omega_s}(\overline{e}_s) \equiv \iint_{\Omega_s}\overline{e}_s\pi_s\,d\Omega - \int_{\Gamma_s^h}\overline{e}_s\hat{q}_s\,d\Gamma \tag{12}$$

$$p_{\Omega_a}(\overline{e}_a) \equiv \iint_{\Omega_a}\overline{e}_a\pi_a\,d\Omega - \int_{\Gamma_a^h}\overline{e}_a\hat{q}_a\,d\Gamma \tag{13}$$

There is no easy way to find analytical solution to Eq. (5) for complex structural-acoustic problems. However, the numerical solution can be obtained by taking advantages of the conventional FEM techniques. Therefore, after taking finite element discretization and Galerkin approximation using interpolation function

$$e_s^i = \boldsymbol{N}_s^{iT}\boldsymbol{E}_s^i,\ e_a^i = \boldsymbol{N}_a^{iT}\boldsymbol{E}_a^i \tag{14}$$

the approximated energy forms of the variational equation are

$$a_{\Omega_s}(e_s,\overline{e}_s) \approx \sum_{i=1}^{NS}\iint_{\Omega_{si}}\left[\frac{c_g^2}{(\eta_s+\eta_{rad})\omega}\nabla\overline{e}_s\cdot\nabla e_s + (\eta_s+\eta_{rad})\omega\,\overline{e}_s e_s\right]d\Omega = \sum_{i=1}^{NS}\overline{\boldsymbol{E}}_s^{iT}\boldsymbol{K}_s^i\boldsymbol{E}_s^i \tag{15}$$

$$d_{\Omega_a}(e_a,\overline{e}_a) \approx \sum_{i=1}^{NA}\iint_{\Omega_{ai}}\left(\frac{c^2}{\eta_a\omega}\nabla\overline{e}_a\cdot\nabla e_a + \eta_a\omega\,\overline{e}_a e_a\right)d\Omega = \sum_{i=1}^{NA}\overline{\boldsymbol{E}}_a^{iT}\boldsymbol{K}_a^i\boldsymbol{E}_a^i \tag{16}$$

$$\ell_{\Omega_s}(\overline{e}_s) \approx \sum_{i=1}^{NS}\left[\iint_{\Omega_{si}}\overline{e}_s\pi_s\,d\Omega - \int_{\Gamma_{si}^h}\overline{e}_s\hat{q}_s\,d\Gamma\right] = \sum_{i=1}^{NS}\overline{\boldsymbol{E}}_s^{iT}\boldsymbol{F}_s^i \tag{17}$$

$$p_{\Omega_a}(\overline{e}_a) \approx \sum_{i=1}^{NA}\left[\iint_{\Omega_{ai}}\overline{e}_a\pi_a\,d\Omega - \int_{\Gamma_{ai}^h}\overline{e}_a\hat{q}_a\,d\Gamma\right] = \sum_{i=1}^{NA}\overline{\boldsymbol{E}}_a^{iT}\boldsymbol{F}_a^i \tag{18}$$

$$b_{\Gamma_{sa}}(e_s,e_a,\overline{e}_s,\overline{e}_a) \approx \sum_{i=1}^{NJ}\int_{\Gamma_{sai}}\overline{e}_s q_s\,d\Gamma + \sum_{i=1}^{NJ}\int_{\Gamma_{sai}}\overline{e}_a q_a\,d\Gamma = \sum_{i=1}^{NJ}\overline{\boldsymbol{E}}_s^{iT}\boldsymbol{Q}_s^i + \sum_{i=1}^{NJ}\overline{\boldsymbol{E}}_a^{iT}\boldsymbol{Q}_a^i \tag{19}$$

where NS is the number of the structural finite elements, NA is the number of the acoustic finite elements, NJ is the number of the finite elements on the interface between the structural and acoustic domains.

Following an assembly process and imposing the essential boundary conditions, the approximate form of the variational equation becomes

$$\begin{bmatrix}\boldsymbol{K}_s & \boldsymbol{0}\\ \boldsymbol{0} & \boldsymbol{K}_a\end{bmatrix}\begin{Bmatrix}\boldsymbol{E}_s\\ \boldsymbol{E}_a\end{Bmatrix} = \begin{Bmatrix}\boldsymbol{F}_s\\ \boldsymbol{F}_a\end{Bmatrix} - \begin{Bmatrix}\boldsymbol{Q}_s\\ \boldsymbol{Q}_a\end{Bmatrix} \tag{20}$$

where $\boldsymbol{E}_s = \left\{\boldsymbol{E}_s^1\ \boldsymbol{E}_s^2\cdots\boldsymbol{E}_s^{NS}\right\}^T$, $\boldsymbol{E}_a = \left\{\boldsymbol{E}_a^1\ \boldsymbol{E}_a^2\cdots\boldsymbol{E}_a^{NA}\right\}^T$, $\boldsymbol{F}_s = \left\{\boldsymbol{F}_s^1\ \boldsymbol{F}_s^2\cdots\boldsymbol{F}_s^{NS}\right\}^T$, $\boldsymbol{F}_a = \left\{\boldsymbol{F}_a^1\ \boldsymbol{F}_a^2\cdots\boldsymbol{F}_a^{NA}\right\}^T$, $\boldsymbol{Q}_s$ and $\boldsymbol{Q}_a$ are the global mapping of the interface force $\left\{\boldsymbol{Q}_s^1\ \boldsymbol{Q}_s^2\cdots\boldsymbol{Q}_s^{NJ}\right\}^T$ and $\left\{\boldsymbol{Q}_a^1\ \boldsymbol{Q}_a^2\cdots\boldsymbol{Q}_a^{NJ}\right\}^T$.

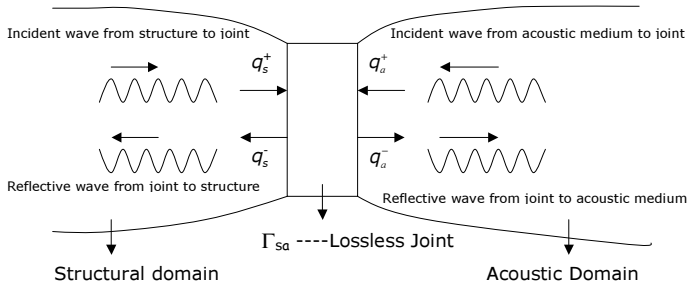

Figure 2. The Power Flow at The Interface Between Structural-Acoustic Domains

The construction of the interface force $\boldsymbol{Q}_s$ and $\boldsymbol{Q}_a$ in Eq. (20) is based on the power flow conservation along the interface Γ_{sa} [23,27]. Consider the coupled structural-acoustic domain in Fig. (2). The net power flow into the structural-acoustic interface Γ_{sa}, denoted by q_s and q_a, are coming respectively from the structural and acoustic domains, and can be written as

$$q_s = q_s^+ - q_s^-,\ q_a = q_a^+ - q_a^- \tag{21}$$

where "+" indicates the incoming power flow to the joint, and "–" indicates the outgoing power flow from the joint. The power flow conservation at the interface requires that $q_s + q_a = 0$. If τ_{sa} is used to represent the power transfer coefficient from *s* to *a* which stands for the structural or acoustic domains, respectively, then the outgoing power flow q_s^- and q_a^- from the joint can be expressed in the form of the incoming power flow q_s^+ and q_a^+, as

$$q_s^- = \tau_{ss} q_s^+ + \tau_{as} q_a^+,\ q_a^- = \tau_{sa} q_s^+ + \tau_{aa} q_a^+ \tag{22}$$

where $\tau_{ss} + \tau_{sa} = 1$ and $\tau_{as} + \tau_{aa} = 1$ are satisfied according to conservation law.

The power flow component can be related with the corresponding energy density component as [35]

$$q_s^+ = c_g e_s^+,\ q_s^- = c_g e_s^-,\ q_a^+ = c e_a^+,\ q_a^- = c e_a^- \tag{23}$$

According to energy superposition, the total time- and space- averaged energy density e_s and e_a at the joint can be expressed in the summation of the incident energy density e_s^+, e_a^+ and the scattered energy density e_s^-, e_a^-, which are carried by the incident wave and the reflective / transmitted wave respectively

$$e_s = e_s^+ + e_s^-, \tag{24.a}$$

$$e_a = e_a^+ + e_a^- \tag{24.b}$$

Premultiply Eq. (24.a) by structural group speed c_g and Eq. (24.b) by air speed c lead to

$$c_g e_s = c_g e_s^+ + c_g e_s^- \tag{25.a}$$

$$c e_a = c e_a^+ + c e_a^- \tag{25.b}$$

Combination of Eq. (21), (22), (23) and (25) establishes the relationship between the power flow and the energy density as

$$\begin{Bmatrix} q_s \\ q_a \end{Bmatrix} = \begin{bmatrix} (1-\tau_{ss}) & -\tau_{as} \\ -\tau_{sa} & (1-\tau_{aa}) \end{bmatrix} \begin{bmatrix} 1+\tau_{ss} & \tau_{as} \\ \tau_{sa} & 1+\tau_{aa} \end{bmatrix}^{-1} \begin{Bmatrix} c_g e_s \\ c e_a \end{Bmatrix} = (\boldsymbol{I} - \boldsymbol{\tau})(\boldsymbol{I} + \boldsymbol{\tau})^{-1} \boldsymbol{c} \begin{Bmatrix} e_s \\ e_a \end{Bmatrix} \tag{26}$$

where $\boldsymbol{\tau} = \begin{bmatrix} \tau_{ss} & \tau_{as} \\ \tau_{sa} & \tau_{aa} \end{bmatrix}$ is the power transfer coefficient matrix, $\boldsymbol{c} = \begin{bmatrix} c_g & 0 \\ 0 & c \end{bmatrix}$ is the group speed matrix and $\boldsymbol{I}$ is a 2 by 2 identity matrix. Thus, the discretized relationship between the power flow and energy density is

$$\begin{Bmatrix} \boldsymbol{Q}_s \\ \boldsymbol{Q}_a \end{Bmatrix} = \begin{Bmatrix} \sum_{i=1}^{NJ} \int_{\Gamma_{sai}} \boldsymbol{N}_s^{iT} \boldsymbol{q}_s^i \, d\Gamma \\ \sum_{i=1}^{NJ} \int_{\Gamma_{sai}} \boldsymbol{N}_a^{iT} \boldsymbol{q}_a^i \, d\Gamma \end{Bmatrix} = \begin{Bmatrix} \sum_{i=1}^{NJ} (\boldsymbol{I} - \boldsymbol{\tau})(\boldsymbol{I} + \boldsymbol{\tau})^{-1} \boldsymbol{c} \begin{Bmatrix} \boldsymbol{N}_s^i & \boldsymbol{N}_a^i \end{Bmatrix}^T \begin{Bmatrix} \boldsymbol{E}_s^i \\ \boldsymbol{E}_a^i \end{Bmatrix} \end{Bmatrix} \equiv \boldsymbol{J}_{sa} \begin{Bmatrix} \boldsymbol{E}_s \\ \boldsymbol{E}_a \end{Bmatrix} \tag{27}$$

With the definition of the junction matrix $\boldsymbol{J}_{sa}$, the global FEM equation of Eq. (20) reduces to

$$\left(\begin{bmatrix} \boldsymbol{K}_s & \boldsymbol{0} \\ \boldsymbol{0} & \boldsymbol{K}_a \end{bmatrix} + \boldsymbol{J}_{sa} \right) \begin{Bmatrix} \boldsymbol{E}_s \\ \boldsymbol{E}_a \end{Bmatrix} = \begin{Bmatrix} \boldsymbol{F}_s \\ \boldsymbol{F}_a \end{Bmatrix} \tag{28}$$

Solving Eq. (28) will yield the energy density in the structural and acoustic domains. From the above derivation, it can be seen that the structural and acoustic stiffness matrices $\boldsymbol{K}_s$ and $\boldsymbol{K}_a$ are symmetric, but the joint matrix $\boldsymbol{J}_{sa}$ is not symmetric because of the fact that the power transfer between the structural and acoustic domains is not reciprocal; i.e., the power transfer coefficient matrix τ is not symmetric. However, as will be shown later in the development of the design sensitivity formulation, the adjoint variable method is also applicable to non-symmetric case.

2.2 Structural-Acoustic Coupling Relationship

The structural-acoustic relationship is expressed in term of the radiation efficiency σ_{rad}, which is defined as the ratio of the acoustic power radiated per unit area of a vibrating surface to the average acoustic power radiated per unit area of a piston that is vibrating with the same average mean square velocity at a frequency for which the piston circumference, exceeds the acoustic wavelength: $kd >> 1$ where d is the radius of the piston. Accordingly, σ_{rad} can be expressed as

$$\sigma_{rad} = \frac{P}{\rho_0 c S \tilde{v}^2} \tag{29}$$

where P is the radiated power, S is the plate surface area, ρ_0 is the fluid density, c is the speed of the sound in fluid, $\tilde{v}^2$ is the averaged mean square velocity.

The radiation efficiency σ_{rad} quantifies the interaction between the structural bending wave and the acoustic wave. A lot of research has been done for accurate numerical evaluation of the radiation efficiency [37,38,39], and in this paper the formulation proposed by Leppington [39] is used:

$$\sigma_{rad}=\begin{cases}\dfrac{a+b}{\pi\mu kab\left(\mu^2-1\right)^{\frac{1}{2}}}\left\{\ln\left(\dfrac{\mu+1}{\mu-1}\right)+\dfrac{2\mu}{\mu^2-1}\right\} & f<f_c\\ \sqrt{\dfrac{a}{\lambda_c}}\left(1+\dfrac{1}{\sqrt{r}}\right) & f\approx f_c\\ \left(1-\dfrac{f_c}{f}\right)^{-\frac{1}{2}} & f>f_c\end{cases} \tag{30}$$

where $r=a/b$ is the ratio between the characteristic length a and b of the plate, $\mu=k_f/k$ is the wave number ratio, $\lambda_c=c/f_c$ is the acoustic wavelength at the coincidence frequency.

For an aluminum plate with the dimension of 1m×1m×0.001m, its capacity to radiate acoustic energy is illustrated in Fig. (3) by the radiation efficiency during the frequency between 100 Hz to 10000 Hz, all below the coincidence frequency, which is 75 kHz. It shows the interaction between the plate and air increases along with the frequency, explaining why the radiation effect needs to be added to the governing equation for high frequency problems.

Based on the radiation efficiency, Bitsie [27] discussed the structural-acoustic coupling and derived the power transfer coefficients between structure (plate) and air, which are expressed as

$$\tau_{sa}=\frac{2\beta\sigma_{rad}}{2+\beta\sigma_{rad}},\ \tau_{ss}=\frac{2-\beta\sigma_{rad}}{2+\beta\sigma_{rad}} \tag{31}$$

where $\beta=c\rho_0/c_s\rho_s$ is the ratio of characteristic impedance.

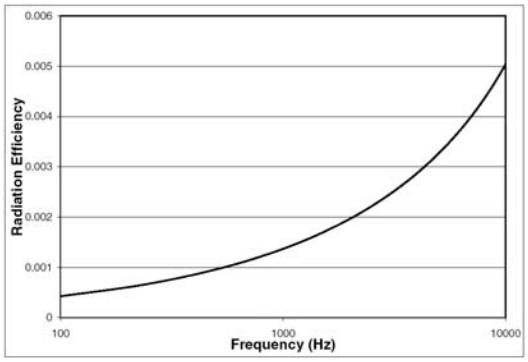

Figure 3. Radiation Efficiency of an Aluminum Plate

For the acoustic-structural coupling, Fahy [40] derived a formula for predicting the capacity of a surface to absorb sound energy as a ratio of the absorbed power to the incident power, which is also expressed in terms of the radiation efficiency as

$$\tau_{as}=\beta\frac{c_0^2}{c_g}\frac{\sigma_{rad}}{fh} \tag{32}$$

As the result of conservation law $\tau_{as}+\tau_{aa}=1$,

$$\tau_{aa}=1-\beta\frac{c_0^2}{c_g}\frac{\sigma_{rad}}{fh} \tag{33}$$

Equations (31)-(33) provide the elements of the power transfer coefficient matrix τ. From the design point of view, the power transfer coefficients are functions of parametric design variables, such as thickness, material properties, etc. With the analytical computation of τ, the EFEM can be used effectively as a design tool by developing and implementing its sensitivity formulation.

3. DESIGN SENSITIVITY ANALYSIS

Design sensitivity is the gradient of a performance measure with respect to design variables, which indicates that how the design change will affect the structural performance. In EFEM, the structural vibrational energy density and acoustic energy density, which are the primary interests in high frequency structural–acoustic problem, usually serve as performance measures. In this paper, parametric design sensitivity analysis is considered, where the parameters of the structural or acoustic property, such as the thickness of a structural panel, hysteresis damping factor, the material property of the structural panel or acoustic medium, etc, are chosen as design variables.

3.1 Definition of a Variation

Given a parametric design variable u, a corresponding performance measure ψ is a function that depends on the design u and $\psi(u)$ is assumed to be continuous with respect to design u. If the design u is perturbed in an arbitrary direction δu with a perturbation size ε, then the variation of $\psi(u)$ in the direction of δu is defined as

$$\psi'_{\delta u}\equiv\frac{d}{d\varepsilon}\psi(u+\varepsilon\delta u)\bigg|_{\varepsilon=0}=\frac{\partial\psi}{\partial u}\delta u \tag{34}$$

If the variation of a function is continuous and linear with respect to δu, then the function is differentiable (more precisely, it is Fréchet differentiable). For complicated problems, it is not easy to prove differentiability of a general function with respect to the design, which is not investigated in this paper.

In this paper, the EFEM primary variables e_s and e_a are assumed to be differentiable. That is, the first variation of e at current design u and in the direction of δu can be written as

$$e'_s=e'_s(\boldsymbol{x};u,\delta u)\equiv\frac{d}{d\varepsilon}e_s(\boldsymbol{x};u+\varepsilon\delta u)\bigg|_{\varepsilon=0} \tag{35}$$

$$e'_a=e'_a(\boldsymbol{x};u,\delta u)\equiv\frac{d}{d\varepsilon}e_a(\boldsymbol{x};u+\varepsilon\delta u)\bigg|_{\varepsilon=0} \tag{36}$$

Based on the differentiability of e_s and e_a, the energy bilinear and load linear forms in the variational Eq. (6) is assumed to be differentiable with respect to the design, which means that their first variations are continuous and linear in δu. Thus, the variations of the energy bilinear and load linear forms are

$$a'_{\delta u}(e_s,\bar{e}_s)\equiv\frac{d}{d\varepsilon}a_{u+\varepsilon\delta u}(\tilde{e}_s,\bar{e}_s)\bigg|_{\varepsilon=0} \tag{37}$$

$$d'_{\delta u}(e_a,\bar{e}_a)\equiv\frac{d}{d\varepsilon}d_{u+\varepsilon\delta u}(\tilde{e}_a,\bar{e}_a)\bigg|_{\varepsilon=0} \tag{38}$$

$$\ell'_{\delta u}(\bar{e}_s)\equiv\frac{d}{d\varepsilon}\ell_{u+\varepsilon\delta u}(\bar{e}_s)\bigg|_{\varepsilon=0} \tag{39}$$

$$p'_{\delta u}(\bar{e}_a)\equiv\frac{d}{d\varepsilon}p_{u+\varepsilon\delta u}(\bar{e}_a)\bigg|_{\varepsilon=0} \tag{40}$$

$$b'_{\delta u}\left(e_s,e_a,\bar{e}_s,\bar{e}_a\right)\equiv\frac{d}{d\varepsilon}b_{u+\delta u}\left(e_s,e_a,\bar{e}_s,\bar{e}_a\right)\bigg|_{\varepsilon=0} \tag{41}$$

Unlike in Section (2), the subscript u is used in the energy bilinear and load linear forms here, instead of the physical

domains as in Eq. (5), to emphasize design dependence of these forms.

In the above expressions, $\bar{e}_s$ and $\bar{e}_a$ are independent of ε and δu, while $\tilde{e}_s$ and $\tilde{e}_a$ denote that the state variables e_s and e_a are being held fixed when the first variation is taken. The subscript δu denotes that the first variation of the energy form is evaluated in the direction of δu.

3.2 Direct Differentiation Method

The variational Eq. (5) can be differentiated with respect to design u to obtain

$$\begin{aligned} &a_u\left(e_s', \bar{e}_s\right) + b_u\left(e_s', e_a', \bar{e}_s, \bar{e}_a\right) + d_u\left(e_a', \bar{e}_a\right) \\ &= \ell'_{\delta u}\left(\bar{e}_s\right) + p'_{\delta u}\left(\bar{e}_a\right) - a'_{\delta u}\left(e_s, \bar{e}_s\right) - b'_{\delta u}\left(e_s, e_a, \bar{e}_s, \bar{e}_a\right) - d'_{\delta u}\left(e_a, \bar{e}_a\right) \end{aligned} \tag{42}$$

Solution to Eq. (42) yields to the variation of the energy density. In the above equation, the left side represents the terms implicitly dependent on the design and the right side are the terms explicitly depending on the design. Comparison of Eq. (42) with the variational Eq. (5) shows that the left side of Eq. (42) has the exactly the same form with Eq. (5) except the argument e_s and e_a are replaced by e_s' and e_a'. Hence, to solve Eq. (42), we can take advantage of the factorized system matrix of Eq. (5) except a different load coming from the contribution from the explicitly dependent terms on the right side.

Generally, a structural–acoustic performance measure can be written in integral form as

$$\psi = \iint_\Omega g(\boldsymbol{e}, \nabla \boldsymbol{e}, u)\, d\Omega \tag{43}$$

where $\boldsymbol{e} = \{e_s \quad e_a\}$, and function g is continuously differentiable with respect to its arguments. Functional in the form of Eq. (43) can be used to represent various structural–acoustic performance measures. For example, the volume integration of energy density represents the total energy in the structure; the integration of product of the Dirac measure with the energy density will recover the energy density at a point; and the power flow can be represented by the integration of product of the group speed and the energy density as well.

The variation of the functional in Eq. (43) is

$$\psi' = \iint_\Omega \left(g_{,u}\delta u + g_{,\boldsymbol{e}} \cdot \boldsymbol{e}' + g_{,\nabla \boldsymbol{e}} : \nabla \boldsymbol{e}' \right) d\Omega \tag{44}$$

Equation (44) is obtained using the fact that $\left(\nabla \boldsymbol{e}\right)' = \nabla \boldsymbol{e}'$, which means that the order of the variation with respect to the design variable and the gradient with respect to the coordinate variable can be interchanged as they are independent to each other [41]. For a given performance measure that can be written in the form of (44), the variation can be readily evaluated using Eq. (44) once the variation of energy density $\boldsymbol{e}'$ is obtained from Eq. (42). In order to compute the variation of the energy density $\boldsymbol{e}'$, the appropriate load vector needs to be constructed based on the terms on the right side of Eq. (42) which are explicitly depending on the design variable u.

In the following section, the plate and air will be considered as design components. For the parametric design sensitivity analysis, the panel thickness, structural material property, structural and acoustic hysteresis damping factors are considered as design parameters. The external loading will be assumed to be independent of design in this paper.

If the structural hysteresis damping factor η_s is used as a design variable, then only $a'_{\delta u}$ in Eq. (5) is related to the design perturbation. As the results, all the explicitly dependent terms on the right side of Eq. (42) will vanish except

$$a'_{\delta \eta_s}(e_s, \bar{e}_s) \equiv \iint_{\Omega_s} \left[-\frac{c_g^2}{\left(\eta_s + \eta_{rad}\right)^2 \omega} \nabla \bar{e}_s \cdot \nabla e_s + \omega \bar{e}_s e_s \right] \delta \eta_s d\Omega \tag{45}$$

Similarly, if the acoustic hysteresis damping factor is used as design variable, then, all the explicitly dependent terms will vanish except

$$d'_{\delta \eta_a}(e_a, \bar{e}_a) \equiv \iint_{\Omega_a} \left(-\frac{c^2}{\eta_a^2 \omega} \nabla \bar{e}_a \cdot \nabla e_a + \omega \bar{e}_a e_a \right) \delta \eta_a \, d\Omega \tag{46}$$

The design changes in damping factors do not affect the structural-acoustic coupling relationship. However, perturbations in the panel thickness and material property will affect the capacity of the plate to radiate the acoustic energy. Thus, not only the energy bilinear form a_u but also the coupling term b_u will be changed due to design change in the panel thickness and material property.

In addition, the energy bilinear form a_u depends on the structural bending group speed and the radiation damping. If the thickness of the plate changes, the variation of the bending group speed is

$$\delta c_g = \frac{1}{2}\left(\frac{D\omega^2}{\alpha \rho_s h}\right)^{-\frac{3}{4}} \left(-\frac{D\omega^2}{\alpha \rho_s h^2}\delta h + \frac{\omega^2}{\alpha \rho_s h}\delta D - \frac{D\omega^2}{\alpha^2 \rho_s h}\delta \alpha \right) \tag{47}$$

where $\delta D = \dfrac{Eh^2}{4\left(1-\nu^2\right)}\delta h$, along with $\delta\alpha$=0 if the frequency ω is above the coincidence frequency and

$$\delta \alpha = -\frac{\rho_0}{\rho_s h^2 \sqrt{k_f^2 - k^2}}\delta h + \frac{4\omega^2 \rho_0}{\rho_s h c_g^3 \sqrt{\left(k_f^2 - k^2\right)^3}}\delta c_g \tag{48}$$

if the frequency ω is below the coincidence frequency.
The variation of the radiation damping defined in Eq. (4) is

$$\delta \eta_{rad} = -\frac{\rho_0 \sigma_{rad}}{\rho_s \alpha k h^2}\delta h - \frac{\rho_0 \sigma_{rad}}{\rho_s \alpha^2 k h}\delta \alpha + \frac{\rho_0}{\rho_s \alpha k h}\delta \sigma_{rad} \tag{49}$$

The variation of the radiation efficiency, which appears in Eq. (49) can be computed according to the Leppington's model in Eq. (30) as

$$\delta \sigma_{rad} = \begin{cases} \left\{ \dfrac{(a+b)}{\pi \mu k a b \left(\mu^2-1\right)^{\frac{1}{2}}} \left[\dfrac{2}{\mu^2-1} + \dfrac{2\left(\mu^2+1\right)}{\left(\mu^2-1\right)^2} \right] + \right. & \\ \left. \dfrac{(a+b)\left(2\mu^2-1\right)}{\pi k a b \mu^2 \left(\mu^2-1\right)^{\frac{3}{2}}} \left[\ln\left(\dfrac{\mu+1}{\mu-1}\right) + \dfrac{2\mu}{\mu^2-1} \right] \right\} \dfrac{2\omega}{c_g^2 k}\delta c_g & f < f_c \\ -\sqrt{\dfrac{a}{\lambda_c^3}}\left(1+\dfrac{1}{\sqrt{r}}\right)\dfrac{c^3}{4\pi f_c^2}\sqrt{\dfrac{12\rho_s\left(1-\nu^2\right)}{E}}\dfrac{1}{h^2}\delta h & f \approx f_c \\ -\left(1-\dfrac{f_c}{f}\right)^{-\frac{3}{2}}\dfrac{c^2}{4\pi f}\sqrt{\dfrac{12\rho_s\left(1-\nu^2\right)}{E}}\dfrac{1}{h^2}\delta h & f > f_c \end{cases} \tag{50}$$

Consequently, the variation of the energy bilinear form a_u is derived as

$$a'_{\delta h}(e_s,\bar{e}_s) \equiv \iint_{\Omega_s}\left[-\frac{c_g^2}{(\eta_s+\eta_{rad})^2\omega}\nabla\bar{e}_s\cdot\nabla e_s\delta\eta_{rad}+\omega\bar{e}_s e_s\delta\eta_{rad} -\frac{2c_g}{(\eta_s+\eta_{rad})\omega}\nabla\bar{e}_s\cdot\nabla e_s\delta c_g\right]d\Omega \tag{51}$$

If the structural thickness and damping design variables perturb simultaneously, the explicitly dependent term of the first variation of the energy bilinear form a_u will be the summation of Eq. (45) and (51), which is $a'_{\delta u}=a'_{\delta\eta_s}+a'_{\delta h}$.

Unlike the energy bilinear form a_u, the variation of the coupling term b_u is difficult to be expressed in continuum form. However, the discrete form of $b'_{\delta u}$ still can be derived from the variation of the joint matrix $\boldsymbol{J}_{sa}$ in Eq. (27) as

$$\begin{aligned}\boldsymbol{J}'_{sa} &= -\boldsymbol{\tau}'\left(\boldsymbol{I}+\boldsymbol{\tau}\right)^{-1}\boldsymbol{c}+\left(\boldsymbol{I}-\boldsymbol{\tau}\right)\left(\boldsymbol{I}+\boldsymbol{\tau}\right)^{-1}\boldsymbol{c}'\\ &\quad-\left(\boldsymbol{I}-\boldsymbol{\tau}\right)\left(\boldsymbol{I}+\boldsymbol{\tau}\right)^{-1}\boldsymbol{\tau}'\left(\boldsymbol{I}+\boldsymbol{\tau}\right)^{-1}\boldsymbol{c}\end{aligned} \tag{52}$$

where $\boldsymbol{c}'=\begin{bmatrix}\delta c_g & 0\\ 0 & 0\end{bmatrix}$ and $\boldsymbol{\tau}'=\begin{bmatrix}\tau'_{ss} & \tau'_{as}\\ \tau'_{sa} & \tau'_{aa}\end{bmatrix}\delta h$, with $\tau'_{ij}=\dfrac{\partial\tau_{ij}}{\partial h}$

which can be obtained from Eqs. (31)-(33). Matrices $\boldsymbol{c}'$ and τ' are the variation of the group speed matrix and the power transfer coefficient matrix correspondingly.

Thus, the variation $b'_{\delta u}$ of the coupling term in terms of the finite element discretization becomes

$$b'_{\delta u}(e_s,e_a,\bar{e}_s,\bar{e}_a)\approx\left\{\bar{\boldsymbol{E}}_s\ \bar{\boldsymbol{E}}_a\right\}^T\boldsymbol{J}'_{sa}\begin{Bmatrix}\boldsymbol{E}_s\\ \boldsymbol{E}_a\end{Bmatrix} \tag{53}$$

Similarly, the continuum variations in Eqs. (45), (46) and (51) of the energy bilinear forms can be approximated by finite element discretization as

$$a'_{\delta u}(e_s,\bar{e}_s)+d'_{\delta u}(e_a,\bar{e}_a)\approx\left\{\bar{\boldsymbol{E}}_s\ \bar{\boldsymbol{E}}_a\right\}^T\begin{Bmatrix}\boldsymbol{F}_s^{fic}\\ \boldsymbol{F}_a^{fic}\end{Bmatrix}\delta u \tag{54}$$

where the vector $\left\{\boldsymbol{F}_s^{fic}\ \boldsymbol{F}_a^{fic}\right\}^T$ is called the fictitious load, which can be computed based on the variations of the explicitly dependent forms listed in Eqs. (45), (46) and (51).

The discrete form of the direct differentiation in Eq. (42) thus reduces to

$$\left(\begin{bmatrix}\boldsymbol{K}_s & \boldsymbol{0}\\ \boldsymbol{0} & \boldsymbol{K}_a\end{bmatrix}+\boldsymbol{J}_{sa}\right)\begin{Bmatrix}\boldsymbol{E}'_s\\ \boldsymbol{E}'_a\end{Bmatrix}=-\boldsymbol{J}'_{sa}\begin{Bmatrix}\boldsymbol{E}_s\\ \boldsymbol{E}_a\end{Bmatrix}-\begin{Bmatrix}\boldsymbol{F}_s^{fic}\\ \boldsymbol{F}_a^{fic}\end{Bmatrix}\delta u \tag{55}$$

Equation (55) has the exactly the same system matrix as Eq. (28). Thus, the factorized system matrix can be used again to solve for the first variation of the energy density, with a different load vector obtained from the first variation of the joint matrix and energy bilinear forms.

Once the sensitivity of the energy density is obtained, the sensitivity of the performance measure can be obtained by evaluating the integration in Eq. (44) using the FEM shape function and Gaussian quadrature.

3.3 Adjoint Variable Method

The direct differentiation method derived in the previous section is efficient when the number of performance measures is more than the number of the design variables, while adjoint variable method is efficient when the number of performance measure is less than the number of the design variables. In a structural-acoustic problem, the energy densities at certain few points usually serve as the performance measures. In this case, the adjoint variable method is more efficient than the direct differentiation method.

For a given performance measure which can be written in the form of Eq. (43), the first variation of the performance measure in Eq. (44) is comprised of two parts: the first term explicitly depends on design u, but the last two terms are related to design u through the primary variable $\boldsymbol{e}$. The adjoint variable method starts from the definition of an adjoint equation with the adjoint load defined by replacing $\boldsymbol{e}'$ and $\nabla\boldsymbol{e}'$ in the last two terms in Eq. (44) by $\bar{\boldsymbol{\lambda}}$ and $\nabla\bar{\boldsymbol{\lambda}}$, respectively, as

$$a_u\left(\bar{\lambda}_s,\lambda_s\right)+b_u\left(\bar{\lambda}_s,\bar{\lambda}_a,\lambda_s,\lambda_a\right)+d_u\left(\bar{\lambda}_a,\lambda_a\right)=\int_\Omega\left(g_{,\boldsymbol{e}}\cdot\bar{\boldsymbol{\lambda}}+g_{,\nabla\boldsymbol{e}}:\nabla\bar{\boldsymbol{\lambda}}\right)d\Omega \qquad \forall\ \bar{\boldsymbol{\lambda}}\in Z \tag{56}$$

where $\boldsymbol{e}=\left\{e_s\quad e_a\right\}^T$, $\boldsymbol{\lambda}=\left\{\lambda_s\quad\lambda_a\right\}^T$.

Since the adjoint equation is satisfied for arbitrary $\bar{\boldsymbol{\lambda}}\in Z$, it can be evaluated at $\bar{\boldsymbol{\lambda}}=\left\{e'_s\quad e'_a\right\}^T$ to yield

$$a_u\left(e'_s,\lambda_s\right)+b_u\left(e'_s,e'_s,\lambda_s,\lambda_a\right)+d_u\left(e'_s,\lambda_a\right)=\int_\Omega\left(g_{,\boldsymbol{e}}\cdot\boldsymbol{e}'+g_{,\nabla\boldsymbol{e}}:\nabla\boldsymbol{e}'\right)d\Omega \tag{57}$$

Similarly, since Eq. (42) is valid for arbitrary $\bar{\boldsymbol{e}}=\left\{\bar{e}_s,\bar{e}_a\right\}\in Z$, it can be evaluated at $\bar{\boldsymbol{e}}=\left\{\lambda_s\quad\lambda_a\right\}$ to yield

$$\begin{aligned}&a_u\left(e'_s,\lambda_s\right)+b_u\left(e'_s,e'_a,\lambda_s,\lambda_a\right)+d_u\left(e'_a,\lambda_a\right)\\ &=\ell'_{\delta u}\left(\lambda_s\right)+p'_{\delta u}\left(\lambda_a\right)-a'_{\delta u}\left(e_s,\lambda_a\right)-b'_{\delta u}\left(e_s,e_a,\lambda_s,\lambda_a\right)-d'_{\delta u}\left(e_a,\lambda_a\right)\end{aligned} \tag{58}$$

Comparison between Eq. (57) and (58) leads to

$$\begin{aligned}\int_\Omega\left(g_{,\boldsymbol{e}}\cdot\boldsymbol{e}'+g_{,\nabla\boldsymbol{e}}:\nabla\boldsymbol{e}'\right)d\Omega &= \ell'_{\delta u}\left(\lambda_s\right)+p'_{\delta u}\left(\lambda_a\right)\\ &\quad-a'_{\delta u}\left(e_s,\lambda_a\right)-b'_{\delta u}\left(e_s,e_a,\lambda_s,\lambda_a\right)-d'_{\delta u}\left(e_a,\lambda_a\right)\end{aligned} \tag{59}$$

Substitution of Eq. (59) into Eq. (44) leads to the expression of the variation of the performance measure as

$$\begin{aligned}\psi' &= \int_\Omega g_{,u}\delta u d\Omega+\ell'_{\delta u}\left(\lambda_s\right)+p'_{\delta u}\left(\lambda_a\right)\\ &\quad-a'_{\delta u}\left(e_s,\lambda_a\right)-b'_{\delta u}\left(e_s,e_a,\lambda_s,\lambda_a\right)-d'_{\delta u}\left(e_a,\lambda_a\right)\end{aligned} \tag{60}$$

The above expression does not need the information for the sensitivity of primary variable $\boldsymbol{e}$; it only involves the direct relationship of the performance measure ψ with the design variable u, and the domain integration of the primary variable $\boldsymbol{e}$ and the adjoint variable λ.

To obtain the adjoint variables, Eq. (56) is discretized to obtain

$$\left(\begin{bmatrix}\boldsymbol{K}_s & \boldsymbol{0}\\ \boldsymbol{0} & \boldsymbol{K}_a\end{bmatrix}+\boldsymbol{J}_{sa}\right)^T\begin{Bmatrix}\boldsymbol{\Lambda}_s\\ \boldsymbol{\Lambda}_a\end{Bmatrix}=\left\{\boldsymbol{F}^{adj}\right\} \tag{61}$$

where $\boldsymbol{F}^{adj}$ comes from the finite element approximation of the right side of Eq. (56). For example, if the performance measure is the energy density at node i of the FEM model, the corresponding adjoint load will be a unit load at node i.

Equation (60) can be evaluated as

$$\psi'=\int_\Omega g_{,u}\delta u d\Omega-\left\{\boldsymbol{J}'_{sa}\boldsymbol{E}+\boldsymbol{F}^{fic}\right\}^T\boldsymbol{\Lambda} \tag{62}$$

where $\boldsymbol{E}=\{\boldsymbol{E}_s\quad\boldsymbol{E}_a\}^T$ and the fictitious load vector $\boldsymbol{F}^{fic}=\left\{\boldsymbol{F}_s^{fic}\ \boldsymbol{F}_a^{fic}\right\}^T$ is defined in Eq. (54).

Note that the solution Λ to the adjoint Eq. (61) requires solving the equation with the transposed system matrix, which is un-symmetric. However, this difficulty can be overcome once the factorized matrix from the analysis process is kept for further usage. As shown in Eq. (62), the adjoint variable method requires the calculation of the fictitious load $\boldsymbol{F}^{fic}$ and the variation of joint matrix $\boldsymbol{J}'_{sa}$, which appear in the direct differentiation method in Eq. (55). Thus, it requires the same computational efforts as the direct differentiation method, except for the number of matrix equations that need to be solved. The direct differentiation method solves the system of matrix equations according to the number of design variables, while the adjoint variable method solves it according to the number of performance measures.

4. NUMERICAL EXAMPLES

4.1 7-plate Engine Foundation Model

In the literature of energy flow approaches to solve high frequency structural-acoustic problem, a ship engine foundation model has been investigated and studied thoroughly by several researchers. Lyon [36] validated the SEA method by dividing the model into 7 and 12 substructures and studying the significance of the in-plane energy in energy transmission. Vlahopoulos [24] discretized the 7-plate model into finite elements (Fig. 4) and applied EFEM to get same results as Lyon.

In complex structures, the structural-structural coupling exits as well as the structural-acoustic coupling, so in 7-plate model, the structural-structural relationship and its design sensitivity will be carried out to verify accuracy of the proposed sensitivity analysis method. The energy finite element model is comprised of 603 nodes, 480 rectangular elements, and 24 structural-structural joints. There are three types of joints in the model: "L", "T" and "cross". The power transfer coefficients are computed using the method developed by Langley and Heron [22], and the sensitivity calculation is based on Kim et al. [33].

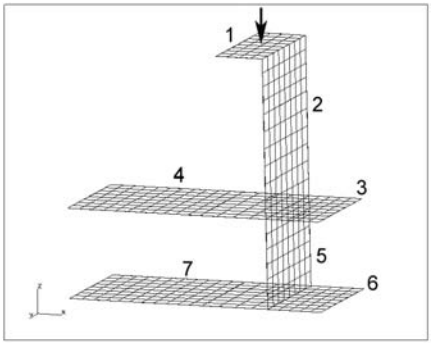

Figure 4. EFEM Model of a 7-plate Ship Engine Foundation

The objective of this example is to verify the sensitivity of the energy ratios between the substructures comparing with the finite difference results. Since calculation of the sensitivity of the energy ratio needs the information of the sensitivity of the energy density of related nodes, the direct differentiation methods is used instead of the adjoint variable method.

A unit power flow input at frequency f=2000 Hz is applied at the center of plate 1. The power flow contributed from each plate is first computed on the frequency average around one third octave band. Figure 5 shows that how the contributions from each substructure to the total power flow will be varied due to the design change in thickness of plate 1, which is allowed to change up to 50% of its initial value, 0.0082m. It can be seen that the thickness change will not only influence its own capacity to dissipate power, but also change the power transfer coefficients between its adjacent plates. The change of power flow distribution can serve as a good reference for design change.

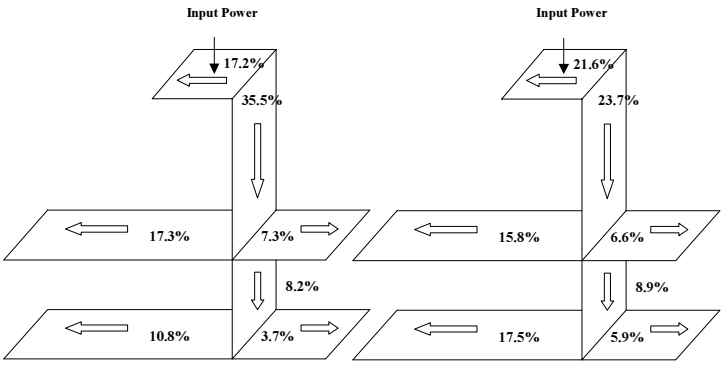

a) Thickness h1=0.0041m b) Thickness h1=0.0123m
Figure 5. Power Flow Distribution at Different Design

The bending energy ratio between the first, fifth and seventh plate are computed by

$$r_{ij} = \frac{E_i}{E_j} = \frac{\sum_i e_i}{\sum_j e_j} \tag{63}$$

Taken the thickness of plate 1 as the design, the sensitivity of the energy ratio can be computed as

$$r'_{ij} = \left(\frac{E_i}{E_j}\right)' = \frac{\left(\sum_i e_i\right)' \sum_j e_j - \sum_i e_i \left(\sum_i e_j\right)'}{\left[\sum_j e_j\right]^2} = \frac{\sum_i e'_i \sum_j e_j - \sum_i e_i \sum_i e'_j}{\left[\sum_j e_j\right]^2} \tag{64}$$

The bending energy ratios between plates 1, 5 and 7 are plotted in Fig. 6. As the thickness of plate 1 increases, the power transfer coefficients from plate 1 to 2 increases, however, due to more energy dissipated in plate 1, the energy ratio of plate 2 over plate 1 still decreases as shown in Fig. 6. Also, in order to compensate the power flow balance in the structure, the energy ratios between plate 5, 7 and plate 1 change correspondingly. Figure 6 provides a good illustration for understanding the energy distribution in the structure due to design change.

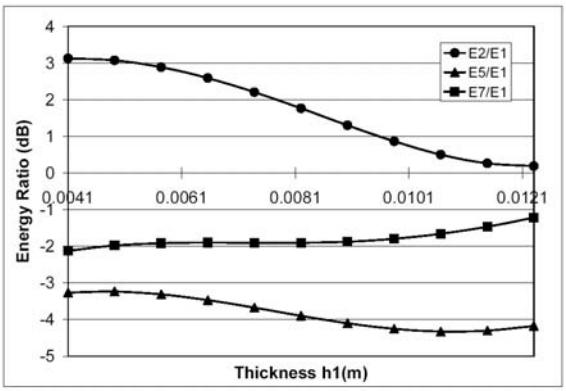

Figure 6. Energy Ratio Due to Design Change in Plate 1

Figure 7 compares the sensitivity results with the finite difference results, where "DDM" stands for Direct Differentiation Method for DSA, "FDM" stands for Finite Difference Method. In this example, the central finite difference method with 1% perturbation is used to compute the sensitivity. Excellent agreement is observed between the two sets of the results to the point that two curves are on top of each other for all energy ratios. It also shows that all the three energy ratios are more sensitive around the initial design (0.0082m).

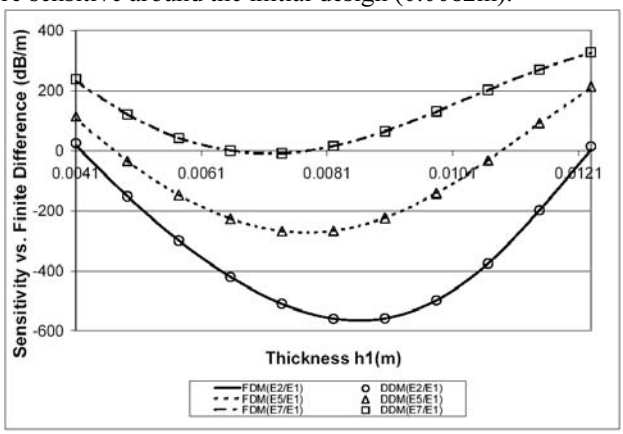

Figure 7. Comparison of Design Sensitivity Results vs. Finite Difference Results

4.2 Simplified Passenger Vehicle Model

A practical application of EFEM is to design a vehicle structure with optimized NVH performance and ride comfort. For this purpose, a simplified passenger vehicle model is constructed and studied (Fig. 8). The corresponding EFEM model (Fig. 9) is comprised of 118 structural plate elements and 92 solid acoustic elements. The sub-structures of the passenger vehicle model are integrated through 56 structural-structural joints and 118 structural-acoustic joints. Choi et al. [8] used the same model to test the proposed sensitivity formulation using FEM for low frequency range.

The passenger vehicle model is comprised of seven different structural panels, made of aluminum. Those panels have the property of Young's modulus E = 71 Gpa, Poisson's ratio ν = 0.33, density ρ_s = 2700 kg/m^3, and all the panels have the same thickness h = 10 mm at initial design; The acoustic space enclosed by the structural panels are filled with air, of density ρ_0 = 1.02 kg/m^3 and wave speed c = 343 m/s.

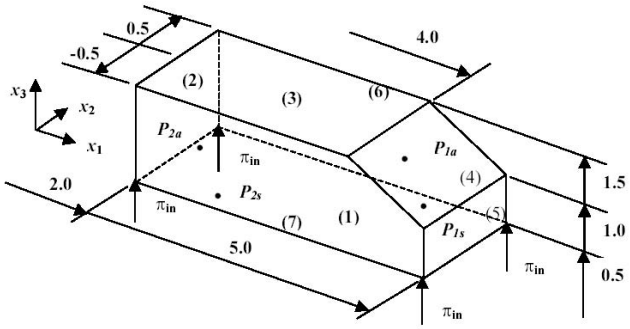

Figure 8. Simplified Passenger Vehicle Model

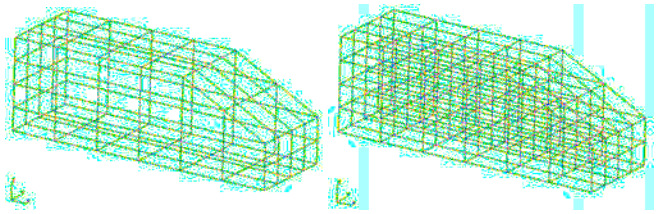
a) Structure part b)Acoustic part

Figure 9. EFEM Model of Simplified Passenger Vehicle

The input power flow is at the four corners, which is obtained from

$$\pi_{in} = \frac{1}{2}|F|^2 \, Real\left(\frac{1}{Z}\right) \tag{65}$$

where F is the magnitude of the input force and Z is the mechanical impedance of the plate. At a high frequency of 5000 Hz, if an approximation derived by Cremer and Heckl [35] is used to evaluate the mechanical impedance as $Z=8\omega\rho_s h/k_f^2$, then the input power can be computed from

$$\pi_{in} = \frac{k_f^2 |F|^2}{16\omega\rho_s h} \tag{66}$$

The energy distribution in the acoustic medium is calculated using EFEM based on the frequency average around one third octave band under applied power flow. The acoustic energy is converted to the root mean square acoustic pressure using the approximation $p = c\sqrt{e\rho_0}$. The sound pressure in terms of decibel level is plotted in Fig. 10. Figure 10(a) illustrates the sound pressure at the boundary of the acoustic medium, while Figure 10(b) shows the acoustic pressure at a longitudinal cross section of the acoustic medium. Black color indicates high sound pressure; white color stands for low sound pressure. It can be seen that although the variation for the sound pressure in the acoustic medium is very small, the energy propagation and decay still makes the sound pressure reduce from the boundary to the center.

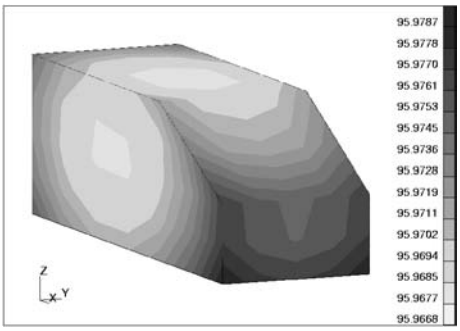

(a) Acoustic Pressure Distribution at the Boundary of the Acoustic Medium

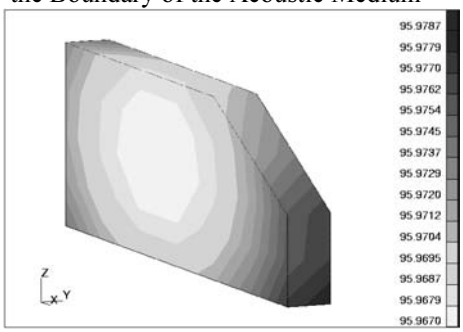

(b) Acoustic Pressure Distribution at a Longitudinal Cross Section of the Acoustic Medium

Figure 10. Interior Noise Distribution in Acoustic Medium by EFEM

Performance measures are chosen as the energy densities at two acoustic points and two structural points, with coordinates at $x_1^a = (4.0,0.25,1.0)$, $x_2^a = (3.0,-0.25,1.0)$, $x_1^s = (4.0,0.25,0.5)$, and $x_2^s = (3.0,-0.25,0.5)$. Thicknesses of selected structural panels are considered as design variables. Adjoint variable method is used to compute the sensitivity coefficients, which are shown in Table 1-3. The central finite difference method with 1% perturbation is used for the finite difference results, which is agreed very well with the sensitivity results. It is noted that when the thickness of panel 1 is chosen as a design variable, the term $\ell'_{\delta u}$ needs to be evaluated since the input power flow computed from Eq. (66) depends on the thickness as well.

Table 1. Sensitivity Results for h1 (Thickness of Panel 1) as Design Variable

Node	$\psi(u-\delta u)$	$\psi(u)$	$\psi(u+\delta u)$	Finite Difference $\Delta\psi$	Sensitivity $\psi/\Delta\varepsilon$	$\Delta\psi/\psi/\Delta\varepsilon$ ×100 (%)
x_1^a	96.0632	95.9687	95.8753	-0.93928E-01	-0.93924E-01	100.0045
x_2^a	96.0617	95.9672	95.8739	-0.93909E-01	-0.93905E-01	100.0045
x_1^s	87.2688	87.1135	86.9597	-0.15452E+00	-0.15452E+00	100.0022
x_2^s	87.2682	87.1129	86.9591	-0.15451E+00	-0.15451E+00	100.0022

Table 2. Sensitivity Results for h3 (Thickness of Panel 3) as Design Variable

Node	$\psi(u-\delta u)$	$\psi(u)$	$\psi(u+\delta u)$	Finite Difference $\Delta\psi$	Sensitivity $\psi/\Delta\varepsilon$	$\Delta\psi/\psi/\Delta\varepsilon$ ×100 (%)
x_1^a	96.0632	95.9685	95.8753	-0.33595E-02	-0.33587E-02	100.0215
x_2^a	96.0617	95.9671	95.8739	-0.34197E-02	-0.34190E-02	100.0214
x_1^s	87.2688	87.0886	86.9597	0.66850E-02	0.66843E-02	100.0106
x_2^s	87.2682	87.0880	86.9591	0.66871E-02	0.66864E-02	100.0106

Table 3. Sensitivity Results for h4 (Thickness of Panel 4) as Design Variable

Node	$\psi(u-\delta u)$	$\psi(u)$	$\psi(u+\delta u)$	Finite Difference $\Delta\psi$	Sensitivity $\psi/\Delta\varepsilon$	$\Delta\psi/\psi/\Delta\varepsilon$ ×100 (%)
x_1^a	95.9705	959685	95.9666	-0.19606E-02	-0.19601E-02	100.0260
x_2^a	95.9690	95.9670	95.9652	-0.18762E-02	-0.18757E-02	100.0265
x_1^s	87.0856	87.0894	87.0932	0.38114E-02	0.38109E-02	100.0131
x_2^s	87.0850	87.0889	87.0926	0.38099E-02	0.38094E-02	100.0132

In order to see the effect of the plate thickness changes, the sensitivity of the sound pressure at the acoustic point x_1^a with respect to the plate thickness is plotted in Figure 11. White color indicates maximum negative sensitivity, and black color indicates minimum negative sensitivity. It can be seen that structural panel 1 has the maximum negative effect to the sound pressure at x_1^a, while the two side panels 6 and 7 have the second largest contribution, which are followed by panel 3 and 4. The sound pressure at x_1^a is least sensitive to the changes of thicknesses of the front and rear panels 2 and 5.

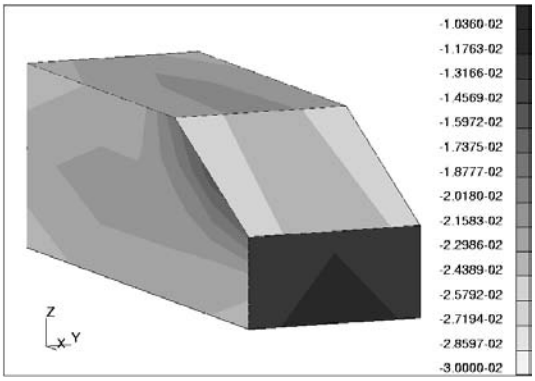

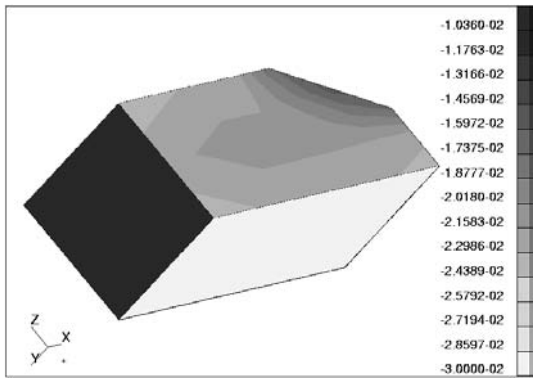

Figure 11. Sensitivity of the Sound Pressure at Point x_1^a with Respect to Thickness

Figure 12 illustrates that dependence of the energy densities at x_1^a and x_1^s on the thickness of panel 1. When the design is ranging 50%-150% of the initial thickness, the sound pressure at x_1^a changes 10.705 dB, corresponding to more than 70% reduction in magnitude. At the same time, the energy density at the structural point x_1^s decreases 16.416 dB, which is equivalent to 97.3% reduction. This indicates that design change in the structural thickness is an effective way to change the performance measure. The DSA results illustrated in Fig. 13 confirm excellent agreement compared with the finite difference results.

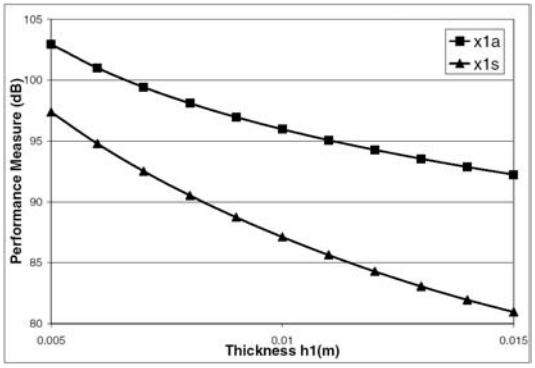

Figure 12. Performance Measures at Observation Points x_1^a and x_1^s with Thickness of Panel 1 as Design Variable

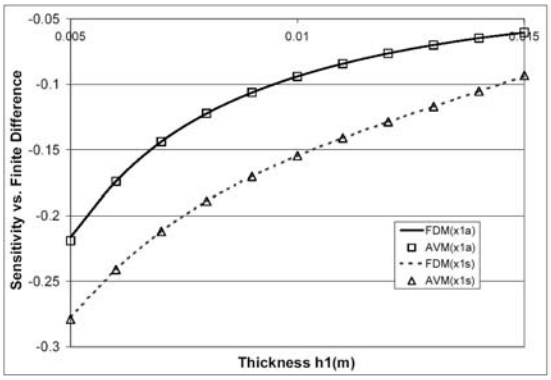

Figure 13. Sensitivity Results for h1 (Thickness of Panel 1) as Design Variable
(AVM--Adjoint variable Method; FDM—Finite Difference Method)

In practical design, dampings of the structure or acoustic medium could serve as design variables. As shown in Fig. 14, the sound pressure at x_1^a changes with the damping factor of panel 1 when the damping of structural panel 1 is ranging ±50% of the initial value (i.e., 0.0005 to 0.0015), the sound pressure at x_1^a will decrease 0.548 dB, which is equivalent to 6.1% reduction. The corresponding sensitivity coefficients are plotted in Fig. 15, which show excellent agreement with the finite difference results. It is interesting to note that the sensitivity coefficients is almost linear in structural damping, implying using material damping as design will be more effective when the damping value is relatively lower.

Table 4. Sensitivity Results for η_1 (Damping of Panel 1) as Design Variable

Node	$\psi(u-\delta u)$	$\psi(u)$	$\psi(u+\delta u)$	Finite Difference $\Delta\psi$	Sensitivity $\psi/\Delta\varepsilon$	$\Delta\psi/\psi/\Delta\varepsilon$ ×100 (%)
x_1^a	95.9739	95.9684	95.9630	-0.54734E-02	-0.54734E-02	100.0001
x_2^a	95.9725	95.9670	95.9615	-0.54734E-02	-0.54734E-02	100.0001
x_1^s	87.0961	87.0905	87.0850	-0.55452E-02	-0.55452E-02	100.0001
x_2^s	87.0955	87.0899	87.0844	-0.55492E-02	-0.55492E-02	100.0001

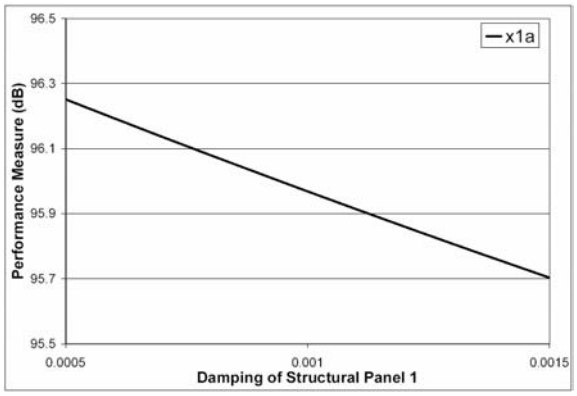

Figure 14. Performance Measure at Observation Points x_1^a with Damping of Panel 1 as Design Variable

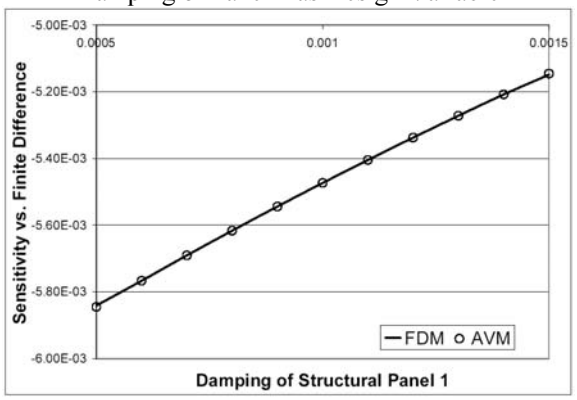

Figure 15. Sensitivity Results: Damping of Panel 1 as Design Variable

As most of the energy dissipation occurs near the power excitation, the thickness of the structural panel which carries the power input will most significantly influence the performance measure. Choosing the structural damping of the excitation panel as design, though, may not be as effective as the structural thickness of the excitation panel. However, it is still more effective than the design variables that are the thicknesses of other panels. Figure 16 shows the sensitivity of the sound pressure at x_1^a with respect to the structural damping. Similar to the sensitivity with respect to the thickness, structural panel 1 has the highest sensitivity, followed by panel 4, panels 6, 7 and 3. The front and rear panels (2 and 5) contribute the lowest sensitivity. Comparing Table 1 through Table 4, it is interesting to note that the contribution from damping, although, is smaller than the contribution from the thickness of panel 1, it is still higher than other structural panel thicknesses. Thus, when the design modification is considered, the thickness change of panel 1 is the most effective, followed by the damping change in the different panels, and then the thickness change in other structural panels.

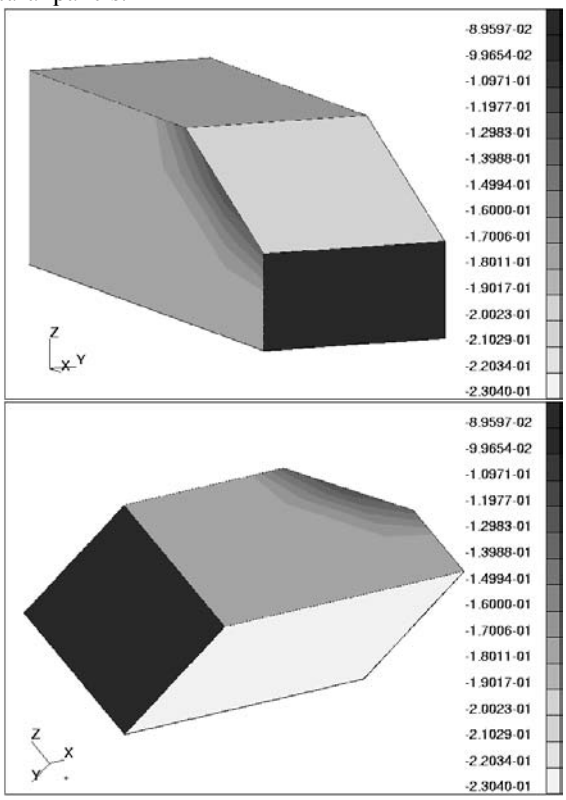

Figure 16. Sensitivity of the Sound Pressure at Point x_1^a with Respect to Damping

The sensitivity information provides the design engineer directions to improve the design. For example, in order to reduce the energy density around point x_1^a, increasing the thickness of structural panel 1 may be the most effective way to do because the thickness change will affect not only the structural radiation damping, but also change the structural-acoustic coupling relationship. On the other hand, changing the damping in panels will not influence the structural-acoustic power transfer coefficients. However, higher damping will help reduce the energy concentration at observation points. Eventually, the DSA information can be utilized by a gradient-based optimization algorithm to search for optimum design.

5. SUMMARY

A continuum approach of computing the sensitivity for high frequency structural-acoustic problem using EFEM is developed and presented. The structural-acoustic coupling relationship characterized by radiation efficiency is carefully reviewed for the purpose of DSA development. Both the direct differentiation and adjoint variable methods are considered where the sensitivity formulation is developed in continuum form and the variation of structural-acoustic coupling relationship is derived from discrete form. Two numerical examples, the 7-plate ship engine foundation model and simplified passenger vehicle model are considered for numerical testing, and sensitivity results demonstrate excellent agreements comparing with the finite difference results and provide a direction for design modification and design optimization.

6. ACKNOWLEDGEMENT

This research is supported by the Automotive Research Center that is sponsored by the US Army TARDEC under contract DAAE07–94–C–R094. The authors gratefully acknowledge this support.

REFERENCES

[1] N. Atalla, R. J. Bernhard, Review of Numerical Solutions for Low-Frequency Structural-Acoustic Problems, Applied Acoustics, 43 (3): 271-294 1994.

[2] T. L. Richards, S. K. Jha, Simplified Finite Element Method For Studying Acoustic Characteristics Inside a Car Cavity, Journal of Sound and Vibration 63 (1): 61-72 1979.

[3] R. J. Bernhard, B. K. Garder, C. G. Mollo, C. R. Kipp, Prediction of Sound Fields in Cavities Using Boundary-Element Methods, AIAA Journal, Vol 25. No 9, 1176-1183, 1986.

[4] N. Vlahopoulos, A Numerical Structure-Borne Noise Prediction Scheme Based on the Boundary-Element Method, With a New Formulation for the Singular-Integrals, Computers & Structures, 50 (1): 97-109 JAN 3 1994.

[5] S. Kopuz, N. Lalor, Analysis of Interior Acoustic Fields Using The Finite Element Method and the Boundary Element Method, Applied Acoustics 45 (3): 193-210 1995.

[6] Z. D. Ma, I. Hagiwara, Development of Eigenmode and Frequency Response Sensitivity Analysis Methods for Coupled Acoustic-Structural Systems, JSME International Journal, Series III, Vol. 35, No. 2, 1995, pp 229-235.

[7] D. C. Smith, R. J. Bernhard, Computation of Acoustic Shape Shape Design Sensitivity Using A Boundary Element Method, Journal of Vibration and Acoustics-Transactions of The ASME, 114 (1): 127-132 JAN 1992.

[8] K. K. Choi, I. Shim, and S. Wang, 1997, Design Sensitivity Analysis of Structure–Induced Noise and Vibration, Journal of Vibration and Acoustics 119(2) 173–179

[9] S. Wang, K. K. Choi, and H. Kulkavni, 1994, Acoustical Optimization of Vehicle Passenger Space, SAE Paper No. 941071.

[10] N. H. Kim, J. Dong, K. K. Choi, N. Vlahopoulos, Z. –D. Ma, M. Castanier, and C. Pierre, 2001, Design Sensitivity Analysis for Sequential Structural–Acoustic Problems, to appear, Journal of Sound and Vibration.
[11] J. Dong, K. K. Choi, N. H. Kim, Design Optimization of Structural-Acoustic Problem Using FEA-BEA with Adjoint Variable Method, Submitted, ASME Journal of Mechanical Design, October 2002.
[12] D. J. Nefske, J. A. Wolf, and L. J. Howell, 1982, Structural–Acoustic Finite Element Analysis of the Automobile Passenger Compartment: A Review of Current Practice, Journal of Sound and Vibration 80(2) 247–266.
[13] R. Lyon, 1975, Statistical Energy Analysis of Dynamical Systems: Theory and Application, The MIT Press, Cambridge, MA.
[14] R. Lyon, G. Maidanik, Power Flow Between Linearly Coupled Oscillators, Journal of Acoustic Society of America, Vol. 34, No. 5, pp 623-639, May 1962.
[15] H. Chen, et al., Statistical Energy Analysis Modeling of a Passenger Vehicle, Proc. Inter-Noise 95, Newport Beach, Ca., 1995, pp.1239-1242.
[16] H. Chen, et al., A Comparison of Test-Based and Analytic SEA Models for Vibro-Acoustics of a Light Truck, Proc. SAE 1995 Noise & Vibration Conf., 951329, 1995, pp. 777-784.
[17] D. J. Nefske and S. H. Sung, 1989, Power Flow Finite–Element Analysis of Dynamic–Systems – Basic Theory and Application to Beams, Journal of Vibration Acoustics Stress and Reliability in Design 111(1) 94–100.
[18] J. Wohlever and R. J. Bernhard, 1992, Mechanical Energy Flow Models of Rods and Beams, Journal of Sound and Vibration 153(1) 1–19.
[19] O. M. Bouthier and R. J. Bernhard, 1992, Models of Space–Averaged Energetics of Plates, AIAA Journal 30(3) 616–623.
[20] O. M. Bouthier and R. J. Bernhard, 1995, Simple–Models of the Energetics of Transversely Vibrating Plates, Journal of Sound and Vibration 182(1) 149–166.
[21] O. M. Bouthier, 1992, Energetics of Vibrating Systems, Ph.D. Thesis, Purdue University.
[22] R. S. Langley and K. H. Heron, 1990, Elastic Wave Transmission through Plate/Beam Junctions, Journal of Vibration and Acoustics 143(2) 241–253.
[23] P. E. Cho, 1993, Energy Flow Analysis of Coupled Structures, Ph.D. Thesis, Purdue University.
[24] N. Vlahopoulos, L. O. Garza-Rios, and C. Mollo, 1999, Numerical Implementation, Validation, and Marine Applications of an Energy Finite Element Formulation, Journal of Ship Research 43(3) 143–156.
[25] W. Zhang, A. Wang, N. Vlahopoulos, Validation of the EFEA Method through Correlation with Conventional FEA and SEA Results, 2001 SAE Noise and Vibration Conference, SAE Paper No. 2001-01-1618.
[26] S. Wang, Theory and Applications of a Simplified Energy Finite Element Method and Its Similarity to SEA, Noise Control Engineering Journal 50 (2): 63-72 MAR-APR 2002.
[27] F. Bitsie, 1996, The Structural–Acoustic Energy Finite Element Method and Energy Boundary Element Method, Ph.D. Thesis, Purdue University.
[28] W. Zhang, A. Wang, N. Vlahopoulos, High Frequency Vibration Analysis of Thin Elastic Plates Under Heavy Fluid Loading by an Energy Finite Element Formulation, Accepted, April 2002, Journal of Sound and Vibration.
[29] R. J. Bernhard, J. Huff, Structural-Acoustic Design at High Frequency Using the Energy Finite Element Method, Journal of Vibration and Acoustics, Transactions of The ASME 1999, Vol 121, Iss 3, pp 295-301.
[30] F. Han, G. Mongeau, and R. J. Bernhard, 1998, Energy Flow Analysis of Beams and Plates for Random Distributed Loading, Journal of Fluids and Structures 12(3) 315–333.
[31] F. Bitsie, R.J. Bernhard, Sensitivity Calculations for Structural-Acoustic EFEM Predictions, Noise Control Engineering, 1998, Vol 46, Iss 3, pp 91-96.
[32] G. A. Borlase and N. Vlahopoulos, 2000, An Energy Finite Element Optimization Process for Reducing High–Frequency Vibration in Large–Scale Structures, Finite Elements in Analysis and Design 36(1) 51–67.
[33] N. H. Kim, J. Dong, K. K. Choi, Energy Flow Analysis and Design Sensitivity Analysis of Structural-Acoustic Problems at High Frequency, Accepted, October 2002, Journal of Sound and Vibration.
[34] J. N. Reddy, Applied Functional Analysis and Variational Methods in Engineering, 1986, MaGraw-Hill, New York, NY.
[35] L. Cremer, L Heckel, and E. E. Ungar, 1988, Structure–Bourn Sound, (second edition), Springer–Verlag, Berlin.
[36] R. Lyon, In-plane Contribution to Structural Noise Transmission, Noise Control Engineering Journal, Jan.-Feb. 1986, pp 22-27.
[37] H. G. Davies, Sound from Turbulent-Boundary-Layer-Excited Panels, The Journal of the Acoustic Society of America 49, 878-889, 1971.
[38] G. Maidanik, Response of Ribbed Panels to Reverberant Acoustic Fields, The Journal of the Acoustic Society of America 34, 809-826, 1962.
[39] F. G. Leppington, E. G. Broadbent, F.R.S., and K. H. Heron, The Acoustic Radiation Efficiency of Rectangular Panels, Proc. R. Soc. Lond., A 382, 245-271, 1982.
[40] F. Fahy, Sound and Structural Vibration: Radiation, Transmission and Response, 1985, Academic Press, London.
[41] E. J. Haug, K. K. Choi, and V. Komkov, Design Sensitivity Analysis of Structural Systems, 1985, Academic Press, New York, NY.